7510 *Inorg. Chem.* **2010**, *49*, 7510–7520
DOI: 10.1021/ic1007473

Inorganic Chemistry
Article

Sulfur-Containing Mixed-Donor Tribenzo-Macrocycles and Their Endo- and Exocyclic Supramolecular Silver(I) and Copper(I) Complexes

Eun-Ju Kang, So Young Lee, Hayan Lee, and Shim Sung Lee*

Department of Chemistry and Research Institute of Natural Science, Gyeongsang National University, Jinju 660-701, South Korea

Received April 19, 2010

New sulfur-containing mixed-donor macrocycles $\mathbf{L^1}$−$\mathbf{L^4}$ with different donor sets and/or ring sizes ($\mathbf{L^1}$, 20-membered O_3S_2; $\mathbf{L^2}$, 20-membered NO_2S_2; $\mathbf{L^3}$, 20-membered O_2S_3; and $\mathbf{L^4}$, 23-membered O_4S_2) were synthesized and structurally characterized by X-ray analysis. A comparative investigation of the coordination behavior of these macrocyclic ligands with silver(I) salts and copper(I) iodide is reported. The X-ray structures of seven complexes (**1**−**7**) have been determined, and a range of structural types and coordination modes, including mono- to multinuclear and endo- to exocyclic ones via M−S bonds, is shown to occur. In all seven complexes, the ether oxygens of each ring are unbound. Reactions of $\mathbf{L^1}$−$\mathbf{L^4}$ with the silver(I) salts (ClO_4^-, BF_4^-, and NO_3^-) afforded four complexes with different topologies: the exocyclic 1-D coordination polymer $[Ag(\mathbf{L^1})(ClO_4)]_n$ (**1**), the endocyclic 1:1 monomer complex $[Ag(\mathbf{L^2})]ClO_4 \cdot CH_3OH$ (**2**), the endo-/exocyclic 1-D coordination polymer $\{[Ag_2(\mathbf{L^2})(CH_3OH)](BF_4)_2\}_n$ (**3**), and the cyclic dimer complex $[Ag_2(\mathbf{L^3})_2(NO_3)_2] \cdot 2CH_3CN$ (**4**). NMR titrations of $\mathbf{L^1}$ and $\mathbf{L^2}$ with silver(I) perchlorate were carried out to explore their complexation behavior in solution and also for comparison with the solid state structures. As well, reaction of the above ligands with copper(I) iodide afforded the exocyclic dimer, $[Cu_2I_2(\mathbf{L^1})_2] \cdot CH_2Cl_2$ (**5**), linked with diamond-type Cu−I_2−Cu unit, the exocyclic monomer complex $[CuI(\mathbf{L^3})] \cdot CH_2Cl_2$ (**6**), and the emissive 1-D poly(cyclic dimer) complex $\{[Cu_4I_4(\mathbf{L^4})_2] \cdot CH_2Cl_2\}_n$ (**7**) linked by a cubane-type Cu_4I_4 unit. The formation of both the discrete and continuous supramolecular complexes with copper(I) iodide is discussed in terms of a ligand-directed "sulfur-to-sulfur" distance effect.

Introduction

Sulfur-donor macrocycles (or thiamacrocycles) often show unusual coordinating behavior toward soft d-block metal ions, giving rise to supramolecular complexes with diverse topologies. Frequently in these, the metal ion is forced to adopt an unusual environment due to exocyclic coordination.[1] For example, such exodentate coordination tends to lead to the formation of coordination polymers with unusual structures, as well as to discrete metallo suprastructures bearing less-common stoichiometries.[2]

We have recently reported that variation of the X donor in O_2S_2X macrocycles (X = S, NH, or O) triggers marked changes in the coordination geometries of the corresponding Ag(I) complexes.[3] Clearly, such behavior reflects the difference in hardness, polarizability, and affinity toward Ag(I) of the different X donors. In view of this, it was of interest to explore the possible related behavior of these ligands toward copper, which in its +1 state also has a d^{10} electronic configuration.[3a] We also proposed that tuning of the sulfur-to-sulfur distance in dithiamacrocycles is effective for discriminating the product because of the different exocoordination modes for silver(I) and mercury(II) ions.[4] The coordination of copper(I) halide with such ligand systems is also of particular interest given the previously documented diverse binding modes displayed by this ion toward dithiamacrocycles and the unique photophysical properties often exhibited by the metal complexes so generated.[5]

*To whom correspondence should be addressed. E-mail: sslee@gnu.ac.kr.

(1) (a) Wolf, R. E., Jr; Hartman, J. R.; Storey, J. M. E.; Foxman, B. M.; Cooper, S. R. *J. Am. Chem. Soc.* **1987**, *109*, 4328. (b) Hill, S. E.; Feller, D. *J. Phys. Chem. A* **2000**, *104*, 652.

(2) (a) Valencia, L.; Pérez-Lourido, P.; Bastida, R.; Macías, A. *Cryst. Growth Des.* **2008**, *8*, 2080. (b) Tiekink, E. R. T.; Vittal, J. J. *Frontiers in Crystal Engineering*; Wiley: Chichester, 2006. (c) Oh, M.; Carpenter, G. B.; Sweigart, D. A. *Acc. Chem. Res.* **2004**, *37*, 1. (d) Lee, S. Y.; Park, S.; Lee, S. S. *Inorg. Chem.* **2009**, *48*, 11335.

(3) (a) Jo, M.; Seo, J.; Seo, M. L.; Choi, K. S.; Cha, S. K.; Lindoy, L. F.; Lee, S. S. *Inorg. Chem.* **2009**, *48*, 8186. (b) Jo, M.; Seo, J.; Lindoy, L. F.; Lee, S. S. *Dalton Trans.* **2009**, 6096. (c) Yoon, I.; Seo, J.; Lee, J.-E.; Song, M. R.; Lee, S. Y.; Choi, K. S.; Jung, O.-S.; Park, K.-M.; Lee, S. S. *Dalton Trans.* **2005**, 2352.

(4) (a) Lee, S. Y.; Park, S.; Kim, H. J.; Jung, J. H.; Lee, S. S. *Inorg. Chem.* **2008**, *47*, 1913. (b) Lee, S. Y.; Seo, J.; Yoon, I.; Kim, C.-S.; Choi, K. S.; Kim, J. S.; Lee, S. S. *Eur. J. Inorg. Chem.* **2006**, 3525. (c) Park, S.; Lee, S. Y.; Jo, M.; Lee, J. Y.; Lee, S. S. *CrystEngComm.* **2009**, *11*, 43.

(5) (a) Lee, J. Y.; Lee, S. Y.; Sim, W.; Park, K.-M.; Kim, J.; Lee, S. S. *Inorg. Chem.* **2008**, *130*, 6902. (b) Graham, P. M.; Pike, R. D. *Inorg. Chem.* **2000**, *39*, 5121. (c) Babich, O. A.; Kokozay, V. N. *Polyhedron* **1997**, *16*, 1487. (d) Vitale, M.; Palke, W. E.; Ford, P. C. *J. Phys. Chem.* **1992**, *96*, 8329. (e) Churchill, M. R.; Rotella, F. J. *Inorg. Chem.* **1977**, *16*, 3267.

Published on Web 07/20/2010

Chart 1. Oxathia- and Azaoxathia-Macrocycles $\mathbf{L^1}-\mathbf{L^4}$ Used in This Work

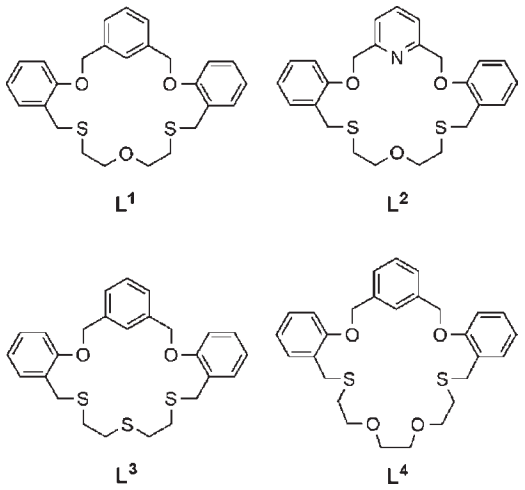

The continuing interest in metallosupramolecular assemblies incorporating thiamacrocyclic systems and the limited research in the area so far has prompted us to investigate the possibility of fabricating new structures of this type. In particular, we were interested in extending the area using some larger thiamacrocycle system with a rigid conformation by employing three aromatic units. Accordingly, the new series of tribenzo-thiaoxa(aza)-macrocycles ($\mathbf{L^1}-\mathbf{L^4}$, Chart 1) was synthesized, and their complexes with silver(I) perchlorate, tetrafluoroborate, and nitrate as well as with copper(I) iodide were prepared and characterized.

Experimental Section

General. All chemicals and solvents used in the syntheses were of reagent grade and were used without further purification. NMR spectra were recorded on a Bruker 300 spectrometer (300 MHz). FT-IR spectra were measured with a VERTEX 80v FT-IR spectrometer. The mass spectra were obtained on a JEOL JMS-700 spectrometer (FAB) and an Applied Biosystems 3200 Q-TRAP (ESI). The elemental analysis was carried out on a LECO CHNS-932 elemental analyzer.

Caution! *The respective perchlorate-containing complexes are potentially explosive, and appropriate precautions should be taken during their preparation, handling, and storage.*

Synthesis and Characterization of $\mathbf{L^1}$. Cesium carbonate (4.21 g, 13.0 mmol) was dissolved in DMF (1000 mL) in a 3 L round-bottom flask. 2-Mercaptoethyl ether (Aldrich, 0.86 g, 6.22 mmol) and dichloride **11a** (2.00 g, 5.20 mmol) were dissolved in DMF (30 mL) and placed in a 50 mL glass syringe. The contents of the syringe were added dropwise at a regular rate (0.6 mL h^{-1}) into the DMF solution under a nitrogen atmosphere with the aid of a microprocessor controlled syringe pump at 45−50 °C over 50 h. The mixture was allowed to stand for a further 10 h. After cooling to room temperature, the reaction mixture was filtered and the solvent evaporated. Water (100 mL) was added, and the mixture was extracted with dichloromethane. The organic phase was dried over anhydrous sodium sulfate and filtered, and the solvent was removed to give a yellow oil. Flash column chromatography (SiO_2, *n*-hexane: ethyl acetate/9:1) afforded the product as a white solid in 57% yield. Mp: 90−92 °C. IR (KBr pellet): 3063, 2927, 2913, 2867, 1597, 1492, 1452, 1234, 1096, 751 cm^{-1}. Anal. Calcd for $[C_{26}H_{28}O_3S_2]$: C, 68.99; H, 6.24. Found: C, 68.87; H, 5.94%. ^{1}H NMR (300 MHz, $CDCl_3$): δ 7.70−6.91 (m, 12H, aromatic), 5.02 (s, 4H, ArCH_2O), 3.79 (s, 4H, ArCH_2S), 3.33 (t, 4H, CH_2CH_2O), 2.51 (t, 4H, CH_2CH_2S). ^{13}C NMR (75 MHz, $CDCl_3$) 156.5, 137.3, 130.7, 128.7, 128.2, 128.1, 127.7, 121.3, 111.8, 70.5, 70.4, 30.9, 30.0. Mass spectrum *m*/*z* (EI): 452.7 $(\mathbf{L^1})^+$.

Synthesis and Characterization of $\mathbf{L^2}$. The synthetic procedure employed was almost the same as that for macrocycle $\mathbf{L^1}$ except for the use of **11b** as the dichloride. Flash column chromatography (SiO_2, *n*-hexane: ethyl acetate/9:1) afforded the product as a white solid in 40% yield. Mp: 125−126 °C. IR (KBr pellet): 3090, 3043, 2929, 2891, 2360, 2329, 1598, 1583, 1491, 1245, 1098, 754 cm^{-1}. Anal. Calcd for $[C_{25}H_{27}NO_3S_2]$: C, 66.20; H, 6.00; N, 3.09. Found: C, 66.17; H, 6.11; N, 2.90%. ^{1}H NMR (300 MHz, $CDCl_3$): δ 7.86−6.94 (m, 11H, aromatic), 5.14 (s, 4H, ArCH_2O), 3.76 (s, 4H, ArCH_2S), 3.14 (t, 4H, OCH_2CH$_2$), 2.40 (t, 4H, CH_2CH_2S). ^{13}C NMR (75 MHz, $CDCl_3$) 156.5, 156.2, 137.6, 130.9, 128.5, 127.9, 122.7, 121.8, 112.2, 71.9, 70.1, 30.3, 29.4. Mass spectrum *m*/*z* (ESI): 454.5 $(\mathbf{L^2}+1)^+$.

Synthesis and Characterization of $\mathbf{L^3}$. The synthetic procedure employed was almost the same as that for macrocycle $\mathbf{L^1}$, except for the use of 2-mercaptoethyl sulfide as the dithiol. Flash column chromatography (SiO_2, *n*-hexane: ethyl acetate/9:1) afforded the product as a white solid in 48% yield. Mp: 101−102 °C. IR (KBr pellet): 3056, 3023, 2930, 2891, 2869, 1594, 1492, 1450, 1236, 1013, 755 cm^{-1}. Anal. Calcd for $[C_{26}H_{28}O_2S_3]$: C, 66.63; H, 6.02. Found: C, 66.43; H, 6.02%. ^{1}H NMR (300 MHz, $CDCl_3$): δ 7.69−6.94 (m, 12H, aromatic), 5.04 (s, 4H, ArCH_2O), 3.78 (s, 4H, ArCH_2S), 2.50, 2.47 (m, overlapped, 8H, SCH_2-CH_2S). ^{13}C NMR (75 MHz, $CDCl_3$): 156.6, 137.3, 130.8, 128.8, 128.5, 128.2, 128.2, 127.6, 121.5, 112.1, 70.6, 32.4, 32.0, 29.9. Mass spectrum *m*/*z* (EI): 468 $(\mathbf{L^4})^+$.

Synthesis and Characterization of $\mathbf{L^4}$. The synthetic procedure was almost the same as that for $\mathbf{L^1}$ except for the use of 2,2′-(ethylenedioxy)diethanethiol as the dithiol. Flash column chromatography (SiO_2; *n*-hexane-ethyl acetate 1:9) afforded the product as a white solid in 41% yield. Mp: 79−80 °C. IR (KBr pellet): 3042, 3011, 2932, 2892, 1705, 1591, 1474, 1451, 1224, 1107, 749, 703 cm^{-1}. Anal. Calcd for $[C_{32}H_{39}O_6S_2]$: C, 65.84; H, 6.73. Found: C, 65.79; H, 6.43%. ^{1}H NMR (300 MHz, $CDCl_3$): δ 7.65−6.90 (m, 12H, aromatic), 5.09 (s, 4H, ArCH_2O), 3.85 (s, 4H, ArCH_2S), 3.49 (t, 4H, OCH_2CH$_2$S), 3.37 (s, 4H, OCH$_2$CH_2O), 2.61 (t, 4H, CH$_2$CH_2S). ^{13}C NMR (75 MHz, $CDCl_3$): 156.5, 137.6, 130.7, 128.7, 128.3, 127.8, 127.2, 126.8, 121.2, 111.9, 70.9, 70.2, 31.1 30.3. Mass spectrum *m*/*z* (EI): 496 $(\mathbf{L^4})^+$.

Preparation of 1, $[\mathbf{Ag(L^1)(ClO_4)}]_n$. Silver perchlorate (4.58 mg, 0.022 mmol) in methanol (2 mL) was added to a solution of $\mathbf{L^1}$ (10.0 mg, 0.022 mmol) in dichloromethane (2 mL). A fine powder, which precipitated from the solution, was filtered off. Vapor diffusion of diethyl ether into the DMF solution gave colorless crystalline product **1** suitable for X-ray analysis (yield: 48%). Mp: 213−215 °C. IR (KBr, pellet): 2925, 2874, 2868, 1599, 1495, 1244, 1107 (ClO_4^-), 1023, 468, 621 cm^{-1}. Anal. Calcd for $[C_{26}H_{30}$-$AgClO_8S_2]$: C, 46.06; H, 4.46; S, 9.46. Found: C, 46.56; H, 4.30; S, 9.47%. Mass spectrum *m*/*z* (ESI): 561.5 $[Ag(\mathbf{L^1})]^+$.

Preparation of 2, $[\mathbf{Ag(L^2)}]\mathbf{ClO_4\cdot CH_3OH}$. Silver perchlorate (9.14 mg, 0.044 mmol) in methanol (2 mL) was added to $\mathbf{L^2}$ (20.0 mg, 0.044 mmol) in dichloromethane (2 mL). The white precipitate that formed was separated and dissolved in acetonitrile. Slow evaporation of the acetonitrile solution afforded crystalline **2** suitable for X-ray analysis (yield: 60%). Mp: 233−234 °C (decomp.). IR (KBr pellet): 3076, 2991, 2940, 2855, 2363, 1703, 1696, 1603, 1490, 1457, 1225, 1108 (ClO_4^-), 1051, 757, 622 cm^{-1}. Anal. Calcd for $[C_{26}H_{29}AgCl_3NO_7S_2]$: C, 41.87; H, 3.92; N, 1.88. Found: C, 41.68; H, 3.67; N, 1.96%. Mass spectrum *m*/*z* (ESI): 560.5 $[Ag(\mathbf{L^2})]^+$.

Preparation of 3, $\{[\mathbf{Ag_2(L^2)(CH_3OH)}](\mathbf{BF_4})_2\}_n$. Silver tetrafluoroborate (8.60 mg, 0.044 mmol) in methanol (2 mL) was added to a solution of $\mathbf{L^2}$ (20.0 mg, 0.044 mmol) in dichloromethane (2 mL). Slow evaporation of the solution afforded colorless crystalline **3** that proved suitable for X-ray analysis (yield: 52%). Mp: 200−201 °C (decomp.). IR (KBr pellet): 3050,

Table 1. Crystal and Experimental Data for $\mathbf{L^1}$, $\mathbf{L^2}$, $\mathbf{L^3}$, and **1**−**7**

	$\mathbf{L^1}$	$\mathbf{L^2}$	$\mathbf{L^3}$	**1**	**2**
formula	$C_{26}H_{26}O_3S_2$	$C_{25}H_{27}NO_3S_2$	$C_{26}H_{28}O_2S_3$	$C_{26}H_{27}AgClO_7S_2$	$C_{26}H_{31}AgClNO_8S_2$
fw	452.60	453.60	468.66	658.92	692.96
temp	296(2)	296(2)	173(2)	296(2)	173(2)
cryst syst	monoclinic	monoclinic	triclinic	monoclinic	monoclinic
space group	$P2_1/c$	$P2_1/n$	$P\bar{1}$	$P2_1/c$	$P2_1/n$
Z	4	4	2	4	4
a (Å)	8.5743(7)	8.6987(5)	8.1947(9)	9.0357(11)	13.5485(12)
b (Å)	8.7776(7)	8.9216(5)	8.2259(10)	16.609(2)	10.9249(9)
c (Å)	30.463(2)	28.6653(15)	18.386(2)	17.374(2)	18.8859(16)
α (deg)	90	90	95.482(2)	90	90
β (deg)	97.707(4)	94.184(3)	91.689(2)	95.371(6)	90.142(2)
γ (deg)	90	90	104.032(2)	90	90
V (Å^3)	2272.0(3)	2218.7(2)	1195.1(2)	2595.9(6)	2795.4(4)
D_{calc} (g/cm^3)	1.323	1.358	1.302	1.686	1.647
absorption coefficient (mm^{-1})	0.260	0.268	0.331	1.086	1.016
cryst size (mm^3)	0.40 × 0.30 × 0.20	0.22 × 0.16 × 0.02	0.24 × 0.20 × 0.15	0.13 × 0.06 × 0.02	0.20 × 0.10 × 0.08
$2\theta_{max}$ (deg)	51.98	56.20	53.00	55.48	52.00
max. and min transmission	0.9498 and 0.9031				0.9231 and 0.8226
R	0.0387	0.0488	0.0649	0.0364	0.0861
wR	0.1024	0.1221	0.1692	0.0933	0.1903
no. of reflections used [>2$\sigma(I)$]	4467 [R(int) = 0.0363]	5405 [R(int) = 0.1420]	4840 [R(int) = 0.0593]	6028 [R(int) = 0.0529]	5488 [R(int) = 0.0667]
diffractometer	Bruker APEX-II CCD	Bruker SMART CCD	Bruker SMART CCD	Bruker APEX-II CCD	Bruker SMART CCD
structure determination	SHELXTL	SHELXTL	SHELXTL	SHELXTL	SHELXTL
refinement	full-matrix	full-matrix	full-matrix	full-matrix	full-matrix

	3	**4**	**5**	**6**	**7**
formula	$C_{26}H_{31}Ag_2B_2F_8NO_4S_2$	$C_{24}H_{22.40}Ag_{0.80}N_{2.40}O_4S_{2.40}$	$C_{26.50}H_{29}ClCuIO_3S_2$	$C_{27}H_{30}C_{12}CuIO_2S_3$	$C_{57}H_{66}Cl_2Cu_4I_4O_8S_4$
fw	875.00	571.68	685.51	744.03	1840.00
temp	173(2)	173(2)	164(2)	100(2)	152(2)
cryst syst	monoclinic	monoclinic	triclinic	orthorhombic	triclinic
space group	$P2_1/c$	$P2_1/c$	$P\bar{1}$	$Pna2_1$	$P\bar{1}$
Z	4	5	4	4	2
a (Å)	11.1076(3)	17.2650(7)	10.6591(5)	20.870(4)	13.5704(14)
b (Å)	14.0306(5)	22.7228(9)	13.2940(7)	6.8790(14)	15.2959(18)
c (Å)	19.8652(6)	8.2636(3)	20.8899(10)	20.667(4)	18.728(2)
α (deg)	90	90	73.689(2)	90	70.101(6)
β (deg)	100.7290(10)	103.506(2)	76.230(2)	90	69.167(6)
γ (deg)	90	90	72.909(2)	90	65.368(6)
V (Å^3)	3041.80(16)	3152.2(2)	2676.3(2)	2967.1(10)	3217.1(6)
D_{calc} (g/cm^3)	1.911	1.506	1.701	1.666	1.899
absorption coefficient (mm^{-1})	1.509	0.881	2.253	2.192	3.486
cryst size (mm^3)	0.27 × 0.10 × 0.06	0.17 × 0.15 × 0.09	0.28 × 0.20 × 0.10	0.05 × 0.04 × 0.01	0.38 × 0.15 × 0.09
$2\theta_{max}$ (deg)	56.66	63.98	55.26	53.00	52.00
max. and min transmission	0.9149 and 0.6861	0.7463 and 0.6270	0.8061 and 0.5711	0.9784 and 0.8983	0.7560 and 0.3509
R	0.0256	0.0603	0.0347	0.0415	0.1075
wR	0.0686	0.1474	0.0933	0.1103	0.2843
no. of reflections used [>2$\sigma(I)$]	7554 [R(int) = 0.0221]	10560 [R(int) = 0.2300]	12296 [R(int) = 0.0428]	3411 [R(int) = 0.0451]	12616 [R(int) = 0.0468]
diffractometer	Bruker APEX-II CCD	Bruker APEX-II CCD	Bruker APEX-II CCD	6BX Bruker Proteum 300	Bruker APEX-II CCD
structure determination	SHELXTL	SHELXTL	SHELXTL	SHELXTL	SHELXTL
refinement	full-matrix	full-matrix	full-matrix	full-matrix	full-matrix

2981, 2955, 2886, 2349, 1702, 1493, 1308, 1091, 1055 (BF_4^-), 1040, 777 cm^{-1}. Anal. Calcd for $[C_{26}H_{31}AgClBF_4NO_4S_2]$: C, 41.57; H, 4.16; N, 1.86. Found: C, 41.90; H, 3.85; N, 1.92%. Mass spectrum m/z (ESI): 561.5 $[Ag(\mathbf{L^2})]^+$.

Preparation of 4, $[Ag_2(\mathbf{L^3})_2(NO_3)_2]\cdot 2CH_3CN$. Silver nitrate (7.25 mg, 0.043 mmol) in methanol (2 mL) was added to $\mathbf{L^3}$ (20 mg, 0.043 mmol) in dichloromethane (2 mL). The colorless precipitate obtained was separated and dissolved in acetonitrile. Slow evaporation of the acetonitrile solution gave crystalline **4** that proved suitable for X-ray analysis (yield: 42%). Mp: 110−111 °C (decomp.). IR (KBr pellet): 3051, 3032, 2920, 2869, 2359, 2340, 1598, 1492, 1453, 1383 (NO_3^-), 1241, 1099, 1046, 1007, 753 cm^{-1}. Anal. Calcd for $[C_{27}H_{30}AgBF_4N_2O_3S_2]$: C, 48.03; H, 4.46; S, 13.74. Found: C, 48.25; H, 4.22; S, 14.19%. Mass spectrum m/z (FAB): 1214.19 $[Ag_2(\mathbf{L^3})_2(NO_3)]^+$.

Preparation of 5, $[Cu_2I_2(\mathbf{L^1})_2]\cdot CH_2Cl_2$. A dichloromethane (2 mL) solution of $\mathbf{L^1}$ (20.0 mg, 0.044 mmol) was allowed to diffuse slowly into an acetonitrile (2 mL) solution of CuI (8.42 mg, 0.044 mmol) in a capillary tube (i.d. 5 mm). Slow evaporation of the solution gave colorless crystalline **5** that proved suitable for X-ray analysis (yield: 62%). Mp: 177−178 °C (decomp.). IR (KBr pellet): 3063, 3034, 2921, 2855, 1597, 1492, 1448, 1386, 1286, 1243, 1153, 1117, 1047, 1021, 763, 733 cm^{-1}. Anal. Calcd for $[C_{26}H_{30}CuIO_4S_2]$: C, 47.24; H, 4.57; S,

Scheme 1. Synthesis of the Macrocyclic Ligands L^1−L^4

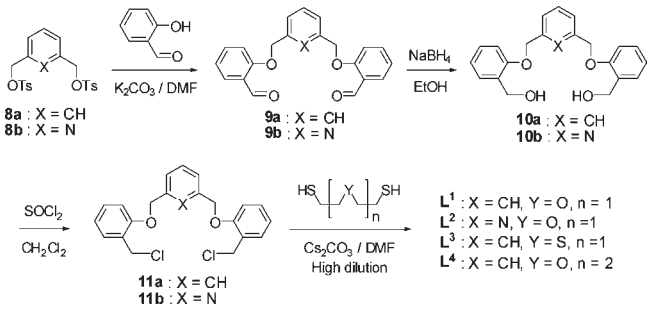

9.70. Found: C, 46.98; H, 4.75; S, 9.99%. Mass spectrum *m*/*z* (ESI): 515.5 $[Cu(L^1)]^+$.

Preparation of 6, $[CuI(L^3)]\cdot CH_2Cl_2$. A dichloromethane (2 mL) solution of L^3 (10.0 mg, 0.021 mmol) was allowed to diffuse slowly into a methanol (2 mL) solution of CuI (4.1 mg, 0.021 mmol) in a capillary tube (i.d. 5 mm). Slow evaporation of the solution gave the colorless crystalline **6** that proved suitable for X-ray analysis (yield: 36%). Mp: 200−201 °C (decomp.). IR (KBr pellet): 3034, 2985, 2918, 2870, 2856, 2353, 2330, 1699, 1597, 1489, 1452, 1403, 1288, 1240, 1099, 1043, 1011, 841, 7490 cm^{-1}. HRMS (FAB) Calcd for $C_{26}H_{28}CuO_2S_3$ $[Cu(L^3)]^+$: 531.0547. Found: 531.0574.

Preparation of 7, $\{[Cu_4I_4(L^4)_2]\cdot CH_2Cl_2\}_n$. A dichloromethane (2 mL) solution of L^4 (20.0 mg, 0.040 mmol) was allowed to diffuse slowly into an acetonitrile (2 mL) solution of CuI (7.67 mg, 0.040 mmol) in a capillary tube (i.d. 5 mm). Slow evaporation of the solution gave colorless crystalline **7** that proved suitable for X-ray analysis (yield: 65%). Mp: 206−208 °C. IR (KBr pellet): 3061, 3033, 2918, 2859, 2358, 2340, 1599, 1495, 1453, 1239, 1102, 1048, 1015, 753, 696, 585 cm^{-1}. HRMS (FAB) Calcd for $C_{28}H_{32}CuO_4S_2$ $[Cu(L^4)]^+$: 559.1038. Found: 559.1055.

X-Ray Crystallographic Analysis. All diffraction data, except that for **6**, were measured at 173 K on a Bruker SMART CCD diffractometer equipped with graphite monochromated Mo Kα radiation (λ = 0.71073 Å). The cell parameters for the compounds were obtained from a least-squares refinement of the spot (from 45 collected frames) using the SMART program. The intensity data were processed using the Saint Plus program. All of the calculations for the structure determination were carried out using the SHELXTL package (version 6.22).[6] Absorption corrections were applied using XPREP and SADABS.[7] Compound **7** shows the relatively high values of *R* and *wR* because of the disorders for S4 and C48 atoms. Crystal data for L^1, L^2, L^3, and **1**−**7** are given in Table 1.

The diffraction data for **6** were measured at 100 K with synchrotron radiation on a 6BX Bruker Proteum 300 CCD detector with a platinum-coated double-crystal monochromator at the Pohang Accelerator Laboratory, Korea. The HKL2000 (v. 0.98.694) software package[8] was used for data collection, cell refinement, reduction, and absorption correction. Collected data were corrected for absorbance using SADABS on the basis of Laue symmetry using equivalent reflections.

Results and Discussion

Syntheses and Characterization of Macrocyclic Ligands L^1−L^4. Synthesis of the target macrocycles involved four steps starting from ditosylates **8** (Scheme 1), with each step proceeding smoothly in reasonable yield. Dichlorides **11** were prepared from the corresponding dialdehydes **9** and dialcohols **10** using a known procedure.[9] L^1−L^4 were commonly obtained by coupling macrocyclization reactions between **11** and the corresponding dithiols in the presence of Cs_2CO_3 under high dilution conditions; again reasonable yields were obtained (L^1, 57%; L^2, 40%; L^3, 48%; L^4, 41%). The ^1H and ^{13}C NMR spectra together with elemental analysis and mass spectra were all in clear agreement with the proposed structures.

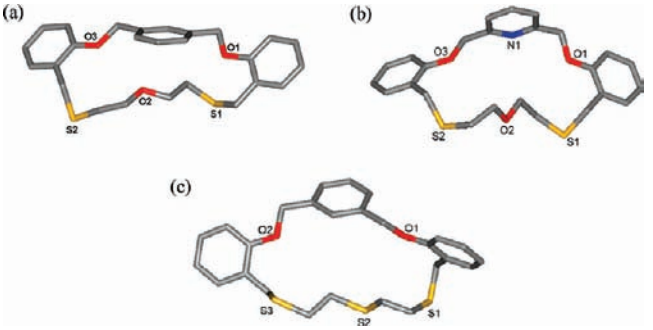

Figure 1. Crystal structures of (a) L^1, (b) L^2, and (c) L^3. Selected torsion angles (deg) between two adjacent donor atoms: for L^1, S1−C−C−O2 = −151.11(63), O2−C−C−S2 = −162.34(41); for L^2, S1−C−C−O2 = −68.36(21), O2−C−C−S2 = −68.95(20); for L^3, S1−C−C−S2 = −174.83(22), S2−C−C−S3 = 174.17(32).

The structures of three of the new macrocycles were also characterized in the solid state by single-crystal X-ray crystallography (Figure 1). Colorless crystals of L^1, L^2, and L^3 suitable for X-ray analysis were obtained by slow evaporation from the solutions of dichloromethane (L^1 and L^3) and methanol (L^2). In each structure, the oxygen atoms adjacent to the center aromatic ring are oriented in an endodentate fashion, while all sulfur atoms are orientated exodentately. L^1 and L^3 have relatively nonfolded configurations in which both of their exodentate sulfur donors are widely separated due to the aliphatic segments between the two adjacent donors being associated with anti arrangements with the torsion angles [for L^1, −151.11(63) and −162.34(41)°; for L^3, −174.83(22) and 174.17(32)]. In L^2, however, the two adjacent donors are associated with gauche arrangements with the torsion angles [−68.36(21) and −68.95(20)]. Accordingly, the respective S···S distances in the macrocycles are 7.649(9) Å for L^1, 6.302(8) Å for L^2, and 8.047(18) Å for L^3.

Preparation and Structures of the Silver(I) Complexes (1−4). On complexation with silver(I) salts (perchlorate, nitrate, and tetrafluoroborate), four new supramolecular complexes (**1**−**4**) were obtained for L^1−L^3 as depicted in Scheme 2. The preparation of the corresponding silver(I) complexes with L^4 was not possible.

Reaction of silver perchlorate with L^1 in methanol/dichloromethane yielded a colorless precipitate. Vapor diffusion of diethyl ether into the DMF solution of the complex gave crystalline **1**. X-ray analysis (Figure 2) of **1** revealed it to have the formula $[Ag(L^1)(ClO_4)]_n$. Selected geometric parameters are presented in Table 2. Interestingly, **1** is an exocoordinated 1-D polymeric species, and

(6) Sheldrick, G. M. *SHELXTL-PC*, version 6.22; Bruker-Analytical X-ray Services: Madison, WI, 2001.

(7) Sheldrick, G. M. *SADABS*; University of Göttingen: Göttingen, Germany, 2000.

(8) Otwinowski, Z.; Minor, W. In *Methods in Enzymology*; Carter, C. W., Jr., Sweet, R. M., Eds.; Academic Press: New York, 1997; Vol. *276*, part A, pp 307−326.

(9) (a) Sultana, K. F.; Lee, S. Y.; Lee, J. Y.; Park, K.-M.; Lee, S. S. *Bull. Korean Chem. Soc.* **2008**, *29*, 241. (b) Sultana, K. F.; Lee, S. Y.; Lee, J.-E.; Seo, J.; Lee, S. S. *Inorg. Chem. Commun.* **2007**, *10*, 1496.

Scheme 2. The Silver(I) Complexes Synthesized in This Study

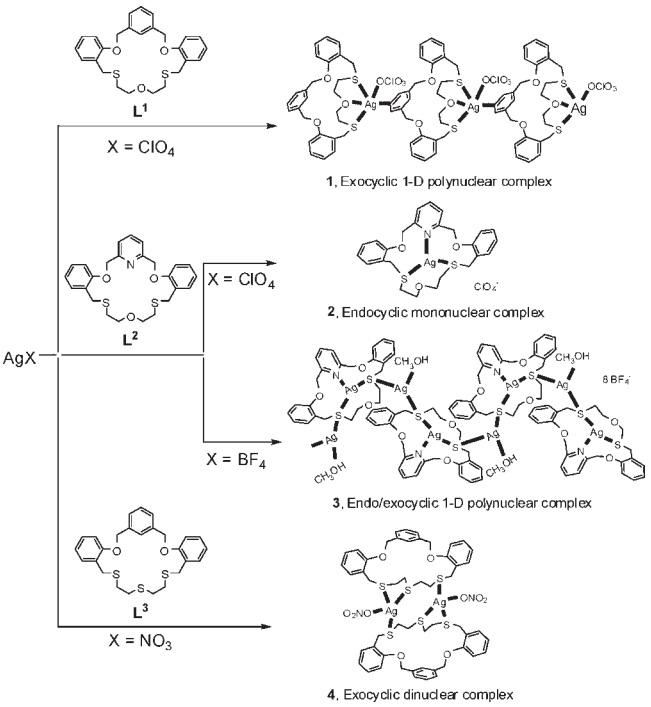

its asymmetric unit contains one **L**, one Ag atom, and one ClO_4^-. Each Ag atom, which lies outside the cavity, is bonded to one O and two S atoms of one macrocycle as well as one aryl carbon atom (C3) from an adjacent $\mathbf{L^1}$, resulting in a $-\mathbf{L^1}-Ag^+-\mathbf{L^1}-Ag^+-$ type 1-D polymeric chain (Figure 2b). The Ag1−C3 distance [2.560(3) Å] lies within the limits (2.47−2.77 Å) reported for such a π bond.[10] The coordination sphere is completed by an O atom from ClO_4^- bound in a monodentate manner with a bond length [Ag1−O4, 2.620(26) Å] that falls within the range observed for other monodentate perchlorate complexes of silver.[4b,10d,11] Thus, the Ag atom is effectively five-coordinate with the coordination geometry best described as a distorted trigonal bipyramid. The S_2C donor atoms define an equatorial trigonal plane [S1−Ag1−C3, 109.94(7); C3−Ag1−S2, 118.29(7); S1−Ag1−S2, 129.35(3)] around the central silver, with axial positions occupied by one ether O atom (O2) and another O atom (O4) from the monodentate ClO_4^- [<O2−Ag1−O4, 158.0(8)°]. The Ag atom is defected out of the trigonal plane by 0.224 Å toward O4. The two oxygen donors (O1 and O3) lying between the aromatic units remain uncoordinated [Ag1···O1, 5.595(21); Ag1···O3, 5.422(20) Å]. It is also noteworthy that the large conformational change in the ligand upon complexation is caused by altering the torsion angles between two adjacent donors, changing from the anti [−151.11(63) and −162.34(41)°] to the gauche form [66.32(30) and −54.69(35)°].

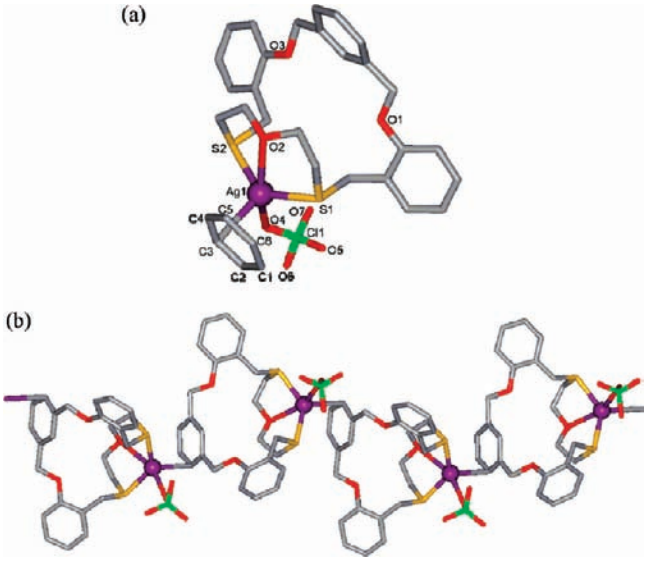

Figure 2. Exocyclic 1-D polymeric structure of **1**, $[Ag(\mathbf{L^1})(ClO_4)]_n$: (a) coordination sphere and (b) 1-D network.

Table 2. Selected Bond Lengths (Å), Bond Angles (deg), and Torsion Angles (deg) for **1**[a]

Ag1−S1	2.487(8)	Ag1−S2	2.486(8)
Ag1−O2	2.710(23)	Ag1−C3A	2.560(3)
Ag1···O4	2.620(26)	Ag1···O1	5.595(21)
Ag1···O3	5.422(20)		
S1−Ag1−S2	129.35(3)	S1−Ag1−O2	74.50(5)
S1−Ag1−O4	85.52(7)	S1−Ag1−C3A	109.94(7)
S2−Ag1−C3A	118.29(7)	S2−Ag1−O2	76.35(6)
S2−Ag1−O4	110.96(6)	O2−Ag1−O4	157.96(8)
S1−C18−C17−O2	66.32(30)	O2−C16−C15−S2	−54.69(35)

[a] Symmetry operation (A): $x, -y + 3/2, z + 1/2$.

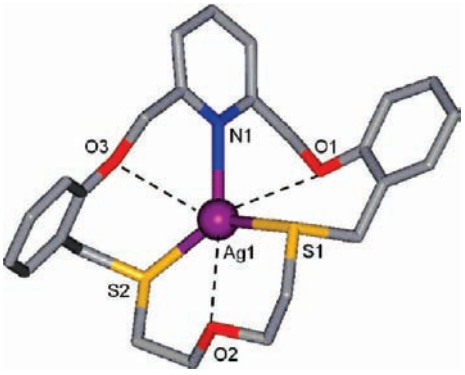

Figure 3. Endocyclic structure of **2**, $[Ag(\mathbf{L^2})]ClO_4 \cdot CH_3OH$. The noncoordinating solvent molecule is omitted for clarity.

The reaction of silver perchlorate with $\mathbf{L^2}$ in methanol/dichloromethane yielded a colorless precipitate which was recrystallized from acetonitrile to give crystalline **2**. X-ray analysis of **2** (Figure 3) revealed it to have the formula $[Ag(\mathbf{L^2})]ClO_4$. The selected geometric parameters are presented in Table 3. In marked contrast to the metal ion position in **1** (derived from $\mathbf{L^1}$), **2** is a typical endocyclic mononuclear complex in which the silver(I) ion has a three-coordinate, trigonal planar geometry with the silver being bound to the two sulfur and one nitrogen

(10) (a) Lee, S. Y.; Jung, J. H.; Vittal, J. J.; Lee, S. S. *Cryst. Growth Des.* **2010**, *10*, 1033. (b) Liddle, B. J.; Hall, D.; Lindeman, S. V.; Smith, M. D.; Gardinier, J. R. *Inorg. Chem.* **2009**, *48*, 8404. (c) Zheng, X.-F.; Zhu, L.-G. *Cryst. Growth Des.* **2009**, *9*, 4407. (d) Kim, H. J.; Lee, S. S. *Inorg. Chem.* **2008**, *47*, 10807. (e) Lee, J.-E.; Lee, J. Y.; Seo, J.; Lee, S. Y.; Kim, H. J.; Park, S. H.; Park, K.-M.; Lindoy, L. F.; Lee, S. S. *Polyhedron* **2008**, *27*, 3004. (f) Lee, J. Y.; Lee, S. Y.; Seo, J.; Park, C. S.; Go, J. N.; Sim, W.; Lee, S. S. *Inorg. Chem.* **2007**, *46*, 6221. (g) Kim, H. J.; Yoon, I.; Lee, S. Y.; Seo, J.; Lee, S. S. *Tetrahedron Lett.* **2007**, *48*, 8464. (h) Munakata, M.; Wu, L. P.; Ning, G. L.; Kuroda-Sowa, T.; Meakawa, M.; Suensga, Y.; Maeno, N. *J. Am. Chem. Soc.* **1999**, *121*, 4968.

(11) Jung, O.-S.; Lee, Y.-A.; Kim, Y. J.; Hong, J. *Cryst. Growth Des.* **2002**, *2*, 497.

Table 3. Selected Bond Lengths (Å), Bond Angles (deg), and Torsion Angles (deg) for **2**

Ag1−N1	2.406(6)	Ag1−S1	2.596(3)
Ag1−S2	2.530(2)	Ag1···O1	3.008(59)
Ag1···O2	2.962(64)	Ag1···O3	2.950(60)
N1−Ag1−S1	101.58(15)	N1−Ag1−S2	118.80(15)
S1−Ag1−S2	139.10(8)		
S1−C17−C16-O2	−68.70(10)	O2−C15−C14−S2	70.88(80)

donor atom of $\mathbf{L^2}$. As might be expected, the pyridine N atom in $\mathbf{L^2}$ appears to bind strongly to the silver center [Ag1−N1, 2.406(6) Å]. The Ag−S bond distances in **2** [Ag1−S1, 2.596(3), Ag1−S2, 2.530(2) Å] are typical but slightly longer than those in **1** (average 2.49 Å). Thus, since **2** shows strong Ag−N(pyridine) bonding, this may contribute to slightly weaker Ag−S bonds in this complex if bond length is taken to be a measure of bond strength. Unlike the coordination of perchlorate in **1**, the perchlorate ion in **2** remains uncoordinated; the preferred anion-free mononuclear endocyclization in **2** presumably reflects the overall strong coordination of the donor set (including, as mentioned above, the pyridine nitrogen atom) of $\mathbf{L^2}$. Additional interactions between the Ag atom and O donors (dashed lines in Figure 3), which are shorter than the sum of the van der Waals radii of Ag and O (3.20 Å), are also present; three ether oxygens [Ag1···O1, 3.008(6); Ag1···O2, 2.962(6); and Ag1···O3, 2.950(6) Å] and one perchlorate oxygen [Ag1···O4, 2.931(11), Supporting Information] interact weakly with the silver.

As mentioned, a comparison of the different coordination modes adopted in **1** and **2** supported the idea that the existence of pyridine as a strong coordinating site in $\mathbf{L^2}$ relative to the presence of an aryl group in $\mathbf{L^1}$ can be a controlling factor influencing exo- (for **1**) versus endocoordination (for **2**) behavior. The preferred endocoordination mode of **2** appears likely to reflect the presence of the strongly bound pyridine unit in $\mathbf{L^2}$, which might be expected to promote the formation of the observed discrete 1:1 species. In contrast, $\mathbf{L^1}$ has no pyridine unit, and instead the π coordination of silver(I) with an the adjacent aryl group occurs, giving rise to the formation of a 1-D network species.

Reaction of silver tetrafluoroborate with $\mathbf{L^2}$ in methanol/dichloromethene afforded colorless crystalline **3** that was suitable for X-ray analysis. Very interestingly, the crystal structure of **3** (Figure 4; Table 4) shows an unusual 1-D arrangement, with the formula being $\{[Ag_2(\mathbf{L^2})(CH_3OH)](BF_4)_2\}_n$. In this structure, successive endocyclic silver(I) complex units are linked with exocyclic silver(I) units via Ag−S bonds, resulting in the observed 1-D network. Selected geometric parameters are presented in Table 3. Similar to the mononuclear endocoordination observed in **2**, the endocyclic Ag1 atom in **3** is bonded to a NS_2 donor set from $\mathbf{L^2}$ in a twisted conformation [S2−C−C−O1, −68.36(21); O1−C−C−S1, −68.95(20)]; three ether oxygens from the macrocycle also interact weakly with silver: Ag1···O1, 2.935(15); Ag1···O2, 3.137(16); and Ag1···O3, 2.772(15) Å. The Ag2 atom outside the cavity bridges the endocyclic Ag1 coordination spheres, resulting in a $[Ag_2(\mathbf{L^1})(CH_3OH)]^+$ repeating unit that repeats via Ag−S bonds. The coordination sphere of Ag2 is completed by a methanol molecule. Accordingly, the local coordination geometry of each Ag atom is distorted trigonal planar, with the "trigonal" angles falling in the range 107.0−130.0° for Ag1 and 111.1−128.1° for Ag2.

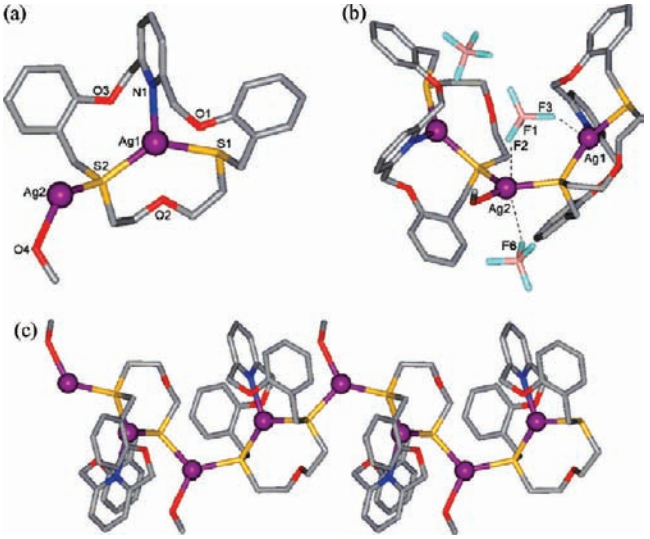

Figure 4. Endo/exocyclic 1-D polymeric structure of **3**, $\{[Ag_2(\mathbf{L^2})(CH_3OH)](BF_4)_2\}_n$: (a) asymmetric unit, (b) side view, and (c) 1-D network. The anions are omitted, except in b.

Table 4. Selected Bond Lengths (Å), Bond Angles (deg), and Torsion Angles (deg) for **3**[a]

Ag1−N1	2.337(17)	Ag1−S1	2.602(5)
Ag1−S2	2.568(5)	Ag2−S2	2.536(6)
Ag2−S1A	2.506(5)	Ag2−O4	2.350(2)
Ag1···O1	2.935(15)	Ag1···O2	3.137(16)
Ag1···O3	2.772(15)	Ag1···F3	2.898(16)
Ag2−F2	2.803(15)	Ag2···F6	2.813(18)
N1−Ag1−S1	106.96(4)	N1−Ag1−S2	122.95(4)
S1−Ag1−S2	129.61(17)	S2−Ag2−O4	128.09(6)
S1A−Ag2−S2	119.88(17)	S1A−Ag2−O4	111.14(7)
S1−C14−C15−O2	68.06(21)	O2−C16−C17−S2	55.03(22)

[a] Symmetry operation (A): $-x+1, y+1/2, -z+1/2$.

Complex **3** is a rare example of a 1-D coordination polymer incorporating both endo- and exocyclic metal ion coordination, with the first example of this type also being reported by us.[12] The formation of such a 1-D network seems to be a consequence of the stabilization of the exocyclic Ag2 coordination sphere relative to that of Ag1. Comparing the bond distances for the endo- and exocyclic silver atoms, it is noteworthy that the Ag−S distances for the exocyclic Ag2 atom [Ag2−S1A, 2.506(5); Ag2−S2, 2.536(6) Å] are shorter than those for the endocyclic Ag1 atom [Ag1−S1, 2.602(5); Ag1−S2, 2.568(5) Å]. Furthermore, the Ag2 atom shows additional interactions to two adjacent BF_4^- ions (Ag2···F, 2.803 and 2.813 Å). Overall, it seems clear that synergic contributions from the ligand, solvent, and anion all contribute toward the stabilization of the observed unique endo/exocyclic coordination behavior of the silver atoms in **3**.

Reaction of silver nitrate with $\mathbf{L^3}$ in methanol/dichloromethane yielded a colorless precipitate. Slow evaporation

(12) (a) Lee, J. Y.; Lee, S. Y.; Park, S.; Kwon, J.; Sim, W.; Lee, S. S. *Inorg. Chem.* **2009**, *48*, 8934. (b) Lee, J. Y.; Kim, H. J.; Jung, J. H.; Sim, W.; Lee, S. S. *J. Am. Chem. Soc.* **2008**, *130*, 13838. (c) Yoon, I.; Seo, J.; Lee, J.-E.; Park, K.-M.; Kim, J. S.; Soo, M.; Lah, M.; Lee, S. S. *Inorg. Chem.* **2006**, *45*, 3487. (d) Heller, M.; Sheldrick, W. S. *Z. Anorg. Allg. Chem.* **2003**, *629*, 1589. (e) Röttgers, T.; Sheldrick, W. S. *Z. Anorg. Allg. Chem.* **2001**, *627*, 1976.

of an acetonitrile solution of this product gave crystals of **4**. The X-ray analysis revealed that **4** is a discrete cyclic dimer of formula $[Ag_2(\mathbf{L}^3)_2(NO_3)_2]\cdot 2CH_3CN$ (see Figure 5). The selected geometric parameters are presented in Table 5. The asymmetric unit contains one $\mathbf{L}^3$, one Ag atom, one coordinated nitrate ion, and one CH_3CN molecule. The structural unit in Figure 5 is generated through an inversion symmetry. The structure consists of a dimeric arrangement in which two macrocycles are sandwiching two silver(I) ions. Each four-coordinated Ag atom lies outside the macrocyclic cavity and is bonded to two S atoms from one $\mathbf{L}^3$ and one S atom from a different $\mathbf{L}^3$. The coordination environment of each silver in **4** is completed by an additional bond to a monodentate nitrato ligand. The "tetrahedral" bond angles around the Ag atom vary from 80.9(7) (O3−Ag1−S3A) to 137.6(3)° (S2−Ag1−S3A). These large deviations of the angles from the regular tetrahedron are due to the formation of the pentagonal rings [Ag1−S2−C−C−S1] via Ag−S bonds together with the steric hindrance between two adjacent ligands linked with a Ag atom. The separation of the two Ag atoms (Ag1···Ag1A, 6.075 Å) is far outside the range expected for an agentophilic interaction. The FAB mass spectrum of **4** contains a peak at m/z 1214, which corresponds to $[Ag_2(\mathbf{L}^3)_2(NO_3)]^+$ as $[M-NO_3-2CH_3CN]^+$; the peak pattern is in agreement with the calculated isotopic pattern for this ion (Figure 6).

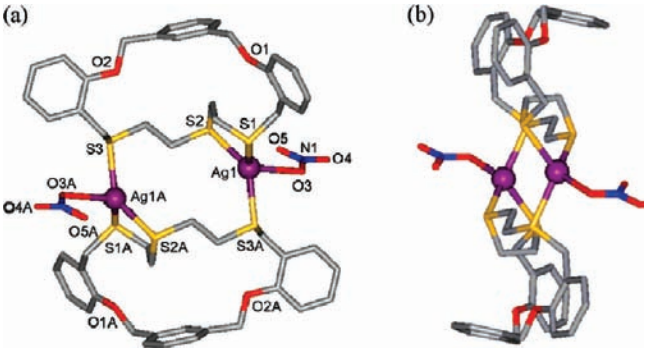

Figure 5. Cyclic dimer structure of **4**, $[Ag_2(\mathbf{L}^3)_2(NO_3)_2]\cdot 2CH_3CN$: (a) front view and (b) side view. The noncoordinating solvent molecules are omitted.

Table 5. Selected Bond Lengths (Å), Bond Angles (deg), and Torsion Angles (deg) for **4**[a]

Ag1−S1	2.654(7)	Ag1−S2	2.542(8)
Ag1−O3	2.497(3)	Ag1−S3A	2.545(8)
S1−Ag1−S2	86.00(2)	S1−Ag1−O3	109.70(7)
S1−Ag1−S3A	115.80(2)	S2−Ag1−S3A	137.64(3)
O3−Ag1−S3A	80.93(7)		
S1−C25−C24−S2	−65.50(27)	S2−C23−C22−S3	−179.93(15)

[a] Symmetry operation (A): $-x+1, -y+1, -z+2$.

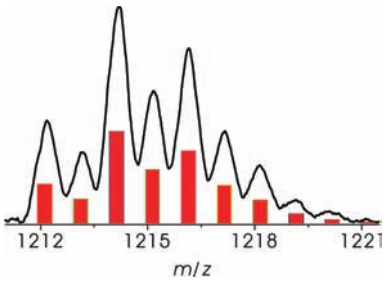

Figure 6. Observed isotope distribution of $[Ag_2(\mathbf{L}^3)_2(NO_3)]^+$ in the FAB mass spectrum of **4**. The bars represent the predicted mass spectral distribution for this ion.

NMR Titration Study of Silver(I) Complexation. As shown in Figures 2 and 3, the two different silver(I) complex structures found for **1** and **2** clearly reflect the different coordination behaviors of the respective macrocycles, reflecting the presence of the benzo ($\mathbf{L}^1$) and pyridine ($\mathbf{L}^2$) subunits. ^{1}H NMR titrations for each silver(I) system were performed in $CD_3CN/CDCl_3$ (1:1) in order to explore the complexation behavior in solution (and also for comparison with the solid state behavior), The signals for the four methylene (H_{1-4}) and the aromatic (H_{a-f}) protons in $\mathbf{L}^1$ and $\mathbf{L}^2$ were well resolved and readily identified (Figures 7a and 8a). Upon stepwise addition of $AgClO_4$ (0−1.5 equiv) to each ligand solution, the signals for all aliphatic protons shifted downfield, in keeping with the occurrence of silver(I) complex formation, with the ligand exchange rate being fast on the NMR time scale.

In both cases, the titration curves (Figures 7b and 8b) show that the plots for all proton signals exhibit no more cation-induced shifts above a molar ratio (Ag/$\mathbf{L}^1$) of 1.0, indicating 1:1 (metal-to-ligand) stoichiometries for the respective complexes, which is same as that observed in the solid state. Above a molar ratio of 1.0, further chemical

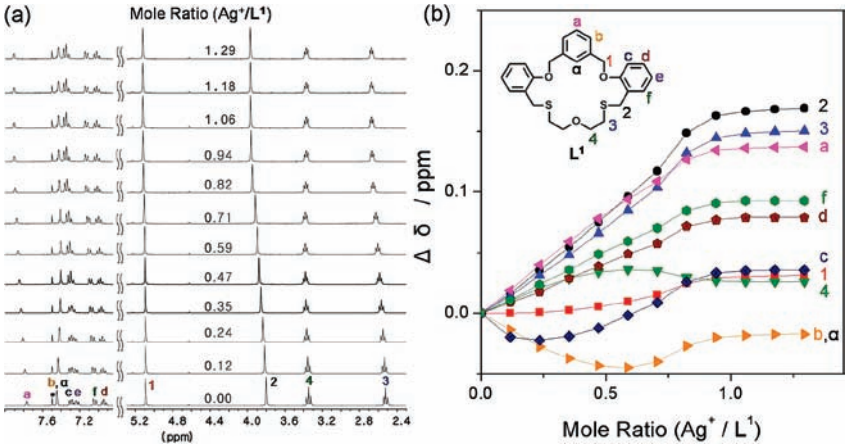

Figure 7. (a) The ^{1}H NMR spectra of $\mathbf{L}^1$ following the stepwise addition of $AgClO_4$ and (b) titration curves for $\mathbf{L}^1$ with $AgClO_4$ in $CD_3CN/CDCl_3$ (1:1).

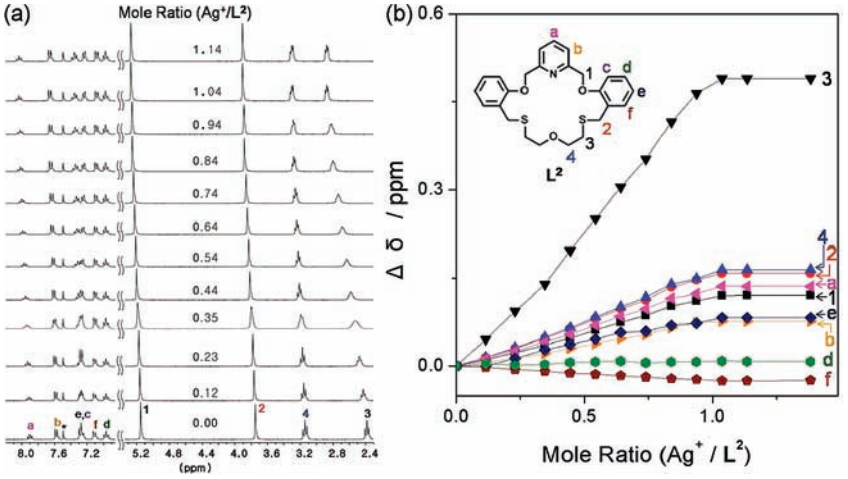

Figure 8. (a) The ^{1}H NMR spectra of $\mathbf{L^2}$ following the stepwise addition of $AgClO_4$ and (b) titration curves for $\mathbf{L^2}$ with $AgClO_4$ in $CD_3CN/CDCl_3$ (1:1).

Scheme 3. Copper(I) Complexes Prepared in the Present Study

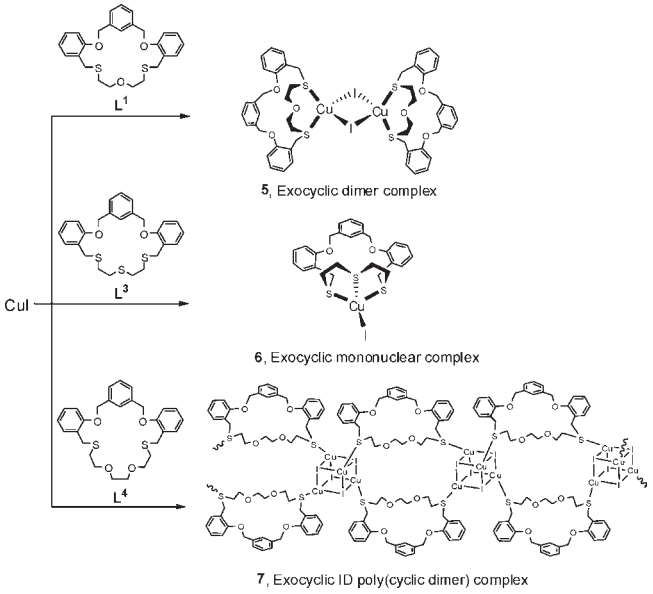

shift changes were negligible. Very notably, the magnitude of the silver(I)-induced chemical shifts ($\Delta\delta$) for the aliphatic protons vary in the sequence: H_2 ($\Delta\delta$: 0.17 ppm) $\geq$ H_3 (0.15 ppm) $\gg$ H_1, H_4 ($\sim$0.04 ppm) for $\mathbf{L^1}$, and H_3 ($\Delta\delta$: 0.49 ppm) $\gg$ H_4, H_2 (0.18 ppm) > H_1 (0.13 ppm) for $\mathbf{L^2}$. The observed larger downfield shifts for the protons adjacent to the S atom relative to those adjacent to oxygen are in accord with silver(I) being strongly bound to the S donor. Furthermore, silver(I) causes a relatively much larger shift for the H_3 peak (0.49 ppm) in $\mathbf{L^2}$ than for the corresponding peak in $\mathbf{L^1}$ (0.15−0.17 ppm), suggesting that the binding modes in these complexes could be different—a result that would parallel the different coordination modes by $\mathbf{L^1}$ and $\mathbf{L^2}$ toward silver(I), as observed in the solid state. In addition, the shift for the aromatic proton H_a (0.14 ppm) in $\mathbf{L^1}$ is much larger than those for the other aromatic protons, perhaps reflecting the presence of a related Ag−π interaction of the type observed in the solid structure of **1**. Consequently, the NMR data suggest that the solution structures of **1** and **2** are in general agreement with those occurring in the solid state.

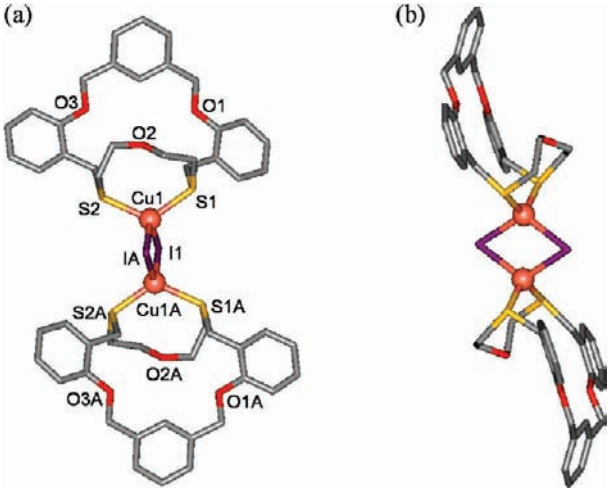

Figure 9. Crystal structure of **5**, $[Cu_2I_2(\mathbf{L^1})_2]\cdot CH_2Cl_2$: (a) front view and (b) side view. The noncoordinating solvent molecule is omitted.

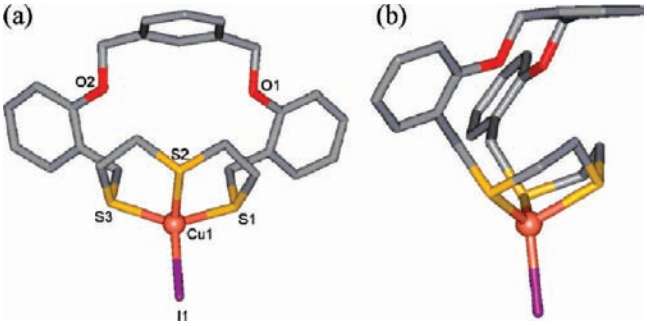

Figure 10. Crystal structure of **6**, $[CuI(\mathbf{L^3})]\cdot CH_2Cl_2$: (a) front view and (b) side view. The noncoordinating solvent molecule is omitted.

Preparation and Structure of the Copper(I) Iodide Complexes (5−7). Having obtained four silver(I) complexes, the coordination products **5**−**7**, showing different topologies, were prepared by the reaction of each ligand with copper(I) iodide, as depicted in Scheme 3, and in each case were structurally characterized by X-ray analysis (Figures 9−11). In this case, the preparation of the copper(I) iodide complex with $\mathbf{L^2}$ was not possible.

A dichloromethane solution of $\mathbf{L^1}$ was allowed to diffuse slowly into an acetonitrile solution of one equivalent

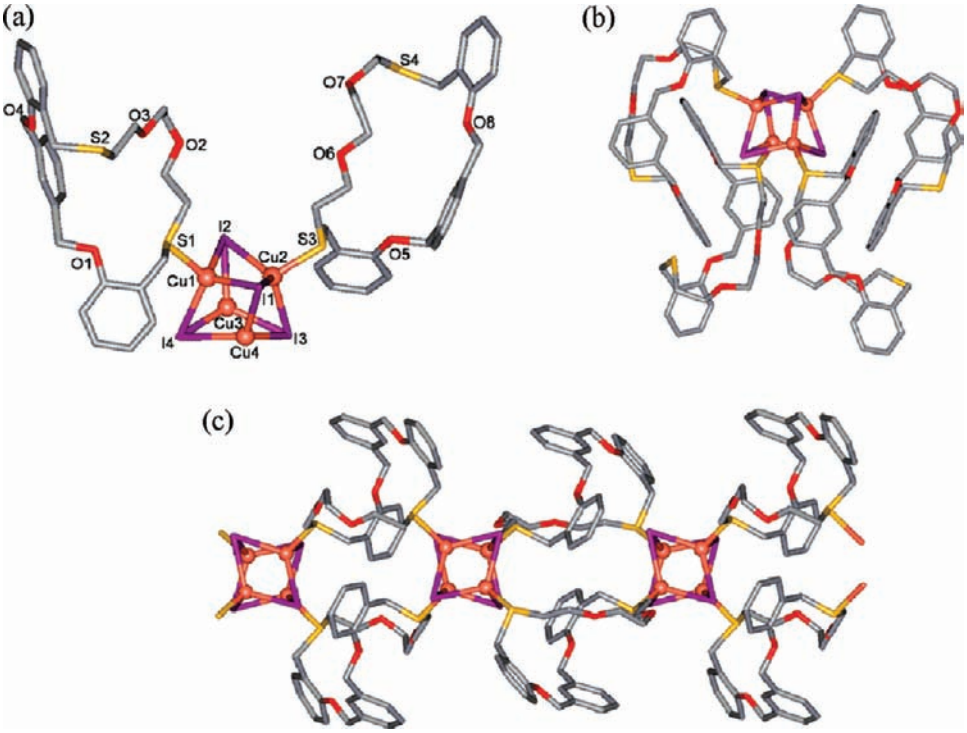

Figure 11. Crystal structure of **7**, $\{[Cu_4I_4(\mathbf{L}^4)_2]\cdot CH_2Cl_2\}_n$: (a) basic coordination unit, (b) coordination environment of the Cu_4I_4−cubane core, and (c) the double-stranded 1-D network. The noncoordinating solvent molecule is omitted.

Table 6. Selected Bond Lengths (Å), Bond Angles (deg), and Torsion Angles (deg) for **5**[a]

Cu1−S1	2.316(9)	Cu1−S2	2.323(8)
Cu1−I1	2.660(5)	Cu1−I1A	2.626(4)
Cu1A-I1	2.626(4)	Cu1−Cu1A	2.802(8)
Cu2−S3	2.291(10)	Cu2−S4	2.304(10)
Cu2−I2	2.706(5)	Cu2−I2A	2.638(5)
Cu2A−I2	2.638(5)	Cu2−Cu2A	2.701(8)
S1−Cu1−S2	120.07(3)	S1−Cu1−I1	98.12(3)
S1−Cu1−I1A	114.14(3)	S2−Cu1−I1	109.01(2)
S2−Cu1−I1A	100.35(2)	I1−Cu1−I1A	115.99(15)
S3−Cu2−S4	121.76(4)	S3−Cu2−I2	101.45(3)
S3−Cu2−I2A	105.04(3)	S4−Cu2−I2	99.50(3)
S4−Cu2−I2A	110.44(3)	I2−Cu2−I2A	119.30(16)
S1−C25−C24−O2	−65.25(33)	O2−C23−C22−S2	−46.92(38)

[a] Symmetry operation (A): $-x+2, -y, -z+1$.

of copper(I) iodide in a capillary tube. As apparently no crystals formed from the diffusion process, crystals of **5** suitable for X-ray analysis were obtained by slow evaporation of a CH_3CN/CH_2Cl_2 solution of the complex. The X-ray structure determination revealed a cofacial dimeric arrangement of formula $[Cu_2I_2(\mathbf{L}^1)_2]\cdot CH_2Cl_2$ (Figure 9); two virtually identical independent dimeric structures are present in the unit cell (Supporting Information). Selected geometric parameters are presented in Table 6. In this structure, two $\mathbf{L}^1$ molecules sandwich an exodentate diamond-like Cu_2I_2 core to form a discrete 2:2:2 (metal/ligand/anion) complex incorporating two Cu−S and two Cu−I bonds to the copper centers. Each copper(I) is four-coordinate, being bound to two exo-oriented sulfur atoms from one macrocycle and the two bridging I atoms. Accordingly, the coordination sphere of the metal center is very distorted tetrahedral, with the "tetrahedral" angles ranging from 98.12(3)° for S1−Cu1−I1 to 120.07(3) for S1−Cu1−S2. In part, the distortion appears to reflect the repulsive interaction between the two sulfur donors in the nine-membered metallacycle formed upon complexation. It could also reflect steric crowding in the nine-membered ring because it has been well established that the bite angle tends to increase with an increase in chelate ring size. Thus, in this case, the metallacycle involving Cu−S bonds seems to be important in the formation of the observed dimeric structure; in this structure, all three O atoms of $\mathbf{L}^1$ remain uncoordinated. Similar to **1**, the large conformational change in the ligand upon complexation is caused mainly by altering the torsion angles between two adjacent donors, changing from the anti [−151.11(63) and −162.34(41)°] to the gauche form [−65.25(33) and −46.92(38)°]. Two cases of related dimeric copper(I) halide complexes of thiamacrocycles with related structures have been reported by us.[2d,3b]

Table 7. Selected Bond Lengths (Å), Bond Angles (deg), and Torsion Angles (deg) for **6**

Cu1−S1	2.303(3)	Cu1−S2	2.364(3)
Cu1−S3	2.290(3)	Cu1−I1	2.554(13)
S1−Cu1−S2	93.68(9)	S1−Cu1−S3	124.35(10)
S1−Cu1−I1	109.15(8)	S2−Cu1−S3	93.96(10)
S2−Cu1−I1	114.52(8)	S3−Cu1−I1	117.04(7)
S1−C15−C16−S2	59.85(94)	S2−C17−C18−S3	−59.26(97)

Colorless single crystals of complex **6** suitable for X-ray analysis were obtained directly from the CH_3CN/CH_2Cl_2 reaction mixture containing $\mathbf{L}^3$ and CuI. The structure of **6** is shown in Figure 10, with selected geometric parameters presented in Table 7. In contrast to **5**, the crystallographic analysis confirms that **6** is a mononuclear complex of formula $[CuI(\mathbf{L}^3)]$. The Cu center is facially coordinated by three S donors from $\mathbf{L}^3$, with the fourth coordination site occupied by an iodide ligand. The two

Table 8. Selected Bond Lengths (Å) and Bond Angles (deg) for **7**

Cu1−S1	2.307(5)	Cu1−I1	2.719(2)
Cu1−I2	2.679(2)	Cu1−I4	2.646(2)
Cu2−S3	2.287(5)	Cu2−I1	2.677(2)
Cu2−I2	2.713(2)	Cu2−I3	2.691(2)
S1−Cu1−I1	105.79(13)	S1−Cu1−I2	102.40(13)
S1−Cu1−I4	110.90(14)	S3−Cu2−I1	106.35(13)
S3−Cu2−I2	106.76(13)	S3−Cu2−I3	102.75(13)
Cu1−I1−Cu2	59.31(7)	Cu1−I2−Cu2	59.35(7)
I1−Cu1−I2	113.86(8)	I1−Cu2−I2	114.13(8)

Chart 2

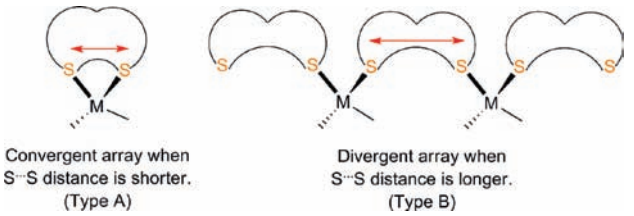

macrocyclic O atoms remain uncoordinated. Again, the coordination sphere of the metal center is distorted tetrahedral; the "tetrahedral" angles range from 93.68(9)° for S1−Cu1−S2 to 124.35(10) for S1−Cu1−S3. The Cu−S bond lengths [2.657(7)−2.760(3) Å] are slightly longer than reported previously for such bonds.[10a,13] Contrasting with this result, we recently reported the preparation and structure of a dimeric copper(I) iodide complex which has similar structure to that of **5** but incorporating a smaller dibenzo-O_2S_3 macrocycle (17-membered) than $\mathbf{L^3}$ (20-membered).[2d,3b] Thus, the preference for mononuclear complex formation may be associated with the greater flexibility of $\mathbf{L^3}$, which allows ready metal coordination to all three consecutive sulfur donors. Thus, the large conformational change observed in the ligand upon complexation is also caused by altering the torsion angles between two adjacent donors, changing from the anti [−174.83(22) and −174.17(32)°] to the gauche form [59.85(94) and −59.26(97)°].

Having successfully obtained two different types of discrete copper(I) iodide complexes of $\mathbf{L^1}$ and $\mathbf{L^3}$, we proceeded to the preparation of a corresponding complex of $\mathbf{L^4}$ incorporating a larger cavity and greater sulfur-to-sulfur distance. Colorless single crystals of **7** (Figure 11 and Table 8) suitable for X-ray analysis were obtained on slow evaporation of the CH_3CN/CH_2Cl_2 reaction mixture containing $\mathbf{L^4}$ and CuI. X-ray analysis revealed that **7** is a rare double-stranded 1-D polymer of type $[Cu_4I_4(\mathbf{L^4})_2]_n$ in which the macrocycles are linked by Cu_4I_4 cores, whose geometry resembles a distorted cube with alternating vertices of Cu and I atoms. Accordingly, the cubane Cu_4I_4 units are located at the center of four $\mathbf{L^4}$ molecules; the four copper atoms in each cluster are tetrahedrally coordinated to three μ_3-iodide atoms and one sulfur donor of $\mathbf{L^4}$. In this case, the four Cu−S bonds between the cubane core and sulfur donors arising from four different ligands occupy well-separated positions, such that the adjacent ligand molecules are also arranged spaciously.

(13) (a) Kim, H. J.; Song, M. R.; Lee, S. Y.; Lee, J. Y.; Lee, S. S. *Eur. J. Inorg. Chem.* **2008**, 3532. (b) Park, K.-M.; Yoon, I.; Seo, J.; Lee, J.-E.; Kim, J.; Choi, K. S.; Jung, O.-S.; Lee, S. S. *Cryst. Growth Des.* **2005**, *5*, 1707. (c) Brooks, N. R.; Brake, A. J.; Champness, N. R.; Cooke, P. A.; Hubberstey, P.; Proserpio, D. M.; Wilson, C.; Schröder, M. *J. Chem. Soc., Dalton Trans.* **2001**, 456.

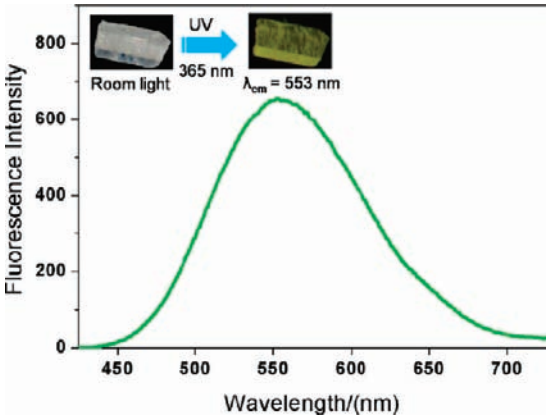

Figure 12. Solid-state photoluminescence spectrum of **7** at room temperature (excitation at 350 nm).

That the polymeric structure of **7** contrasts with those of **5** and **6** is noteworthy in terms of the crystal engineering approach. Recently, we proposed that simple tuning of sulfur-to-sulfur separation in dithiamacrocycles represents a method for controlling the supramolecular structures of resulting soft metal complexes such as mercury[4a,c] and silver.[4b,c,10d] This approach simply means that if the separation between two macrocyclic S donors is small in the macrocyclic cavity, the two S donors will cooperate to chelate to one metal ion (type A; Chart 2). On the other hand, if the separation is larger, each S donor will tend to coordinate to different metal ion centers (type B), leading to the formation of networked species, although other factors may also contribute. Applying this concept to the observed copper(I) iodide complex system in this work, we realize that the longer sulfur-to-sulfur distance in $\mathbf{L^4}$ induces the exobridging coordination (type B) to produce the polymeric network **7** in contrast to **5** and **6**.

Solid-state photoluminescence studies were carried out for **5**−**7** at room temperature. Complexes **5** and **6** were found to be nonemissive. However, **7** exhibits a bright-green emission (λ_{em} = 553 nm) which is likely due to the presence of a cluster-centered excited state with mixed halide-to-metal charge transfer character (see Figure 12).[12b,13a,14]

Conclusion

We have described the synthesis and structural characterization of four sulfur-containing mixed donor macrocycles and their supramolecular complexes with both silver(I) salts and copper(I) iodide. The assembly reactions of the macrocycles with the respective silver(I) salts employed provide a facile means of generating different metallo-supramolecules, including an exocyclic 1-D polymer, an endocyclic mononuclear complex, an endo/exocyclic 1-D polymer, and an exocyclic cyclic dimer. From these results, it may be concluded that the anion-coordination ability and/or the donor variation have important consequences for the resulting topologies of the silver(I) complexes obtained. Parallel reactions with copper(I) iodide also afforded less common products, including an exocyclic dimer, an exocyclic monomer, and a double-stranded 1-D polymer complex. The versatility of the

(14) (a) Sullivan, R. M.; Martin, J. D. *J. Am. Chem. Soc.* **1999**, *121*, 10092. (b) Henary, M.; Wootton, J. L.; Khan, S. I.; Zink, J. I. *Inorg. Chem.* **1997**, *36*, 796. (c) Liu, P.-H.; Zink, J. I. *Inorg. Chem.* **1977**, *16*, 3165.

ligand systems in generating unusual complex structures has been discussed with emphasis in particular cases placed on the influence of the sulfur-to-sulfur distance in controlling the topologies of the resulting products. Our present results clearly show that a small change at the molecular level (building block or reactant) in the assembly system can induce a large change at the supramolecular level (assembled product).

Acknowledgment. This work was supported by WCU project of MEST and NRF. We would like to express our thanks to Prof. L. F. Lindoy (The University of Sydney, Australia) for his helpful advice in preparing manuscript.

Supporting Information Available: Crystallographic data in CIF format and the additional crystal structures. This material is available free of charge via the Internet at http://pubs.acs.org.